

Supplementary Information for

Relative performance of 1-D versus 3-D Hydrodynamic, Water-Quality Models for Predicting Water Temperature and Oxygen in a Shallow, Eutrophic, Managed Reservoir

Xiamei Man ¹, Chengwang Lei ^{1,*}, Cayelan C. Carey ² John C. Little ³

¹ Centre for Wind, Waves and Water, School of Civil Engineering, The University of Sydney, Sydney, NSW 2006, Australia; xman2403@uni.sydney.edu.au

² Department of Biological Sciences, Virginia Tech, Blacksburg, Virginia, USA; cayelan@vt.edu

³ Department of Civil and Environmental Engineering, Virginia Tech, 401 Durham Hall, Blacksburg, Virginia, USA; jcl@vt.edu

* Correspondence: chengwang.lei@sydney.edu.au; Tel.: +61-2-9351-2457

S1. GLM-AED2 time-step dependency test results

Table S1 presents the GLM-AED2 time-step settings, the corresponding computing time and representative results. The model performance is evaluated by the absolute variation relative to the shortest time-step results.

Table S1. GLM-AED2 time-step settings, the corresponding computing time and results.

Time-step (s)	3,600	7,200	21,600	43,200	86,400
Computing time* (s)	0.1	0.05	0.01	0.005	0.002
Average thermocline depth (m)	5.8 ± 0.8	5.6 ± 1.1	5.6 ± 1.1	5.5 ± 0.7	6.4 ± 0.6
Absolute variation** (%)	–	3.4	3.4	5.2	10
Average metalimnion bottom depth (m)	8.6 ± 1.5	8.7 ± 1.2	8.7 ± 1.2	8.2 ± 0.8	8.1 ± 0.1
Absolute variation** (%)	–	1.2	1.2	4.7	5.8

* Wall clock time (Real time) for a one-day simulation using 4× Intel Core i5-4570S CPU @ 2.90GHz.

** The average absolute variation is calculated relative to the 3,600s time-step result.

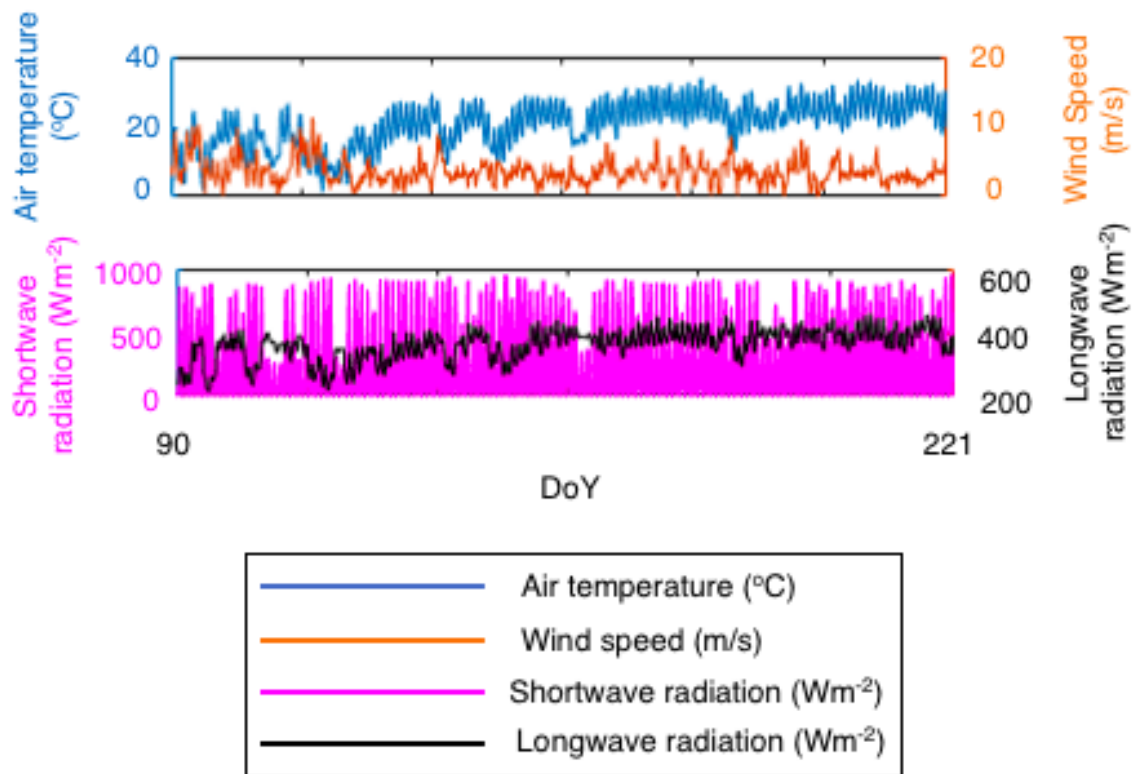


Figure S1. Input meteorological data with 1-hour temporal resolution

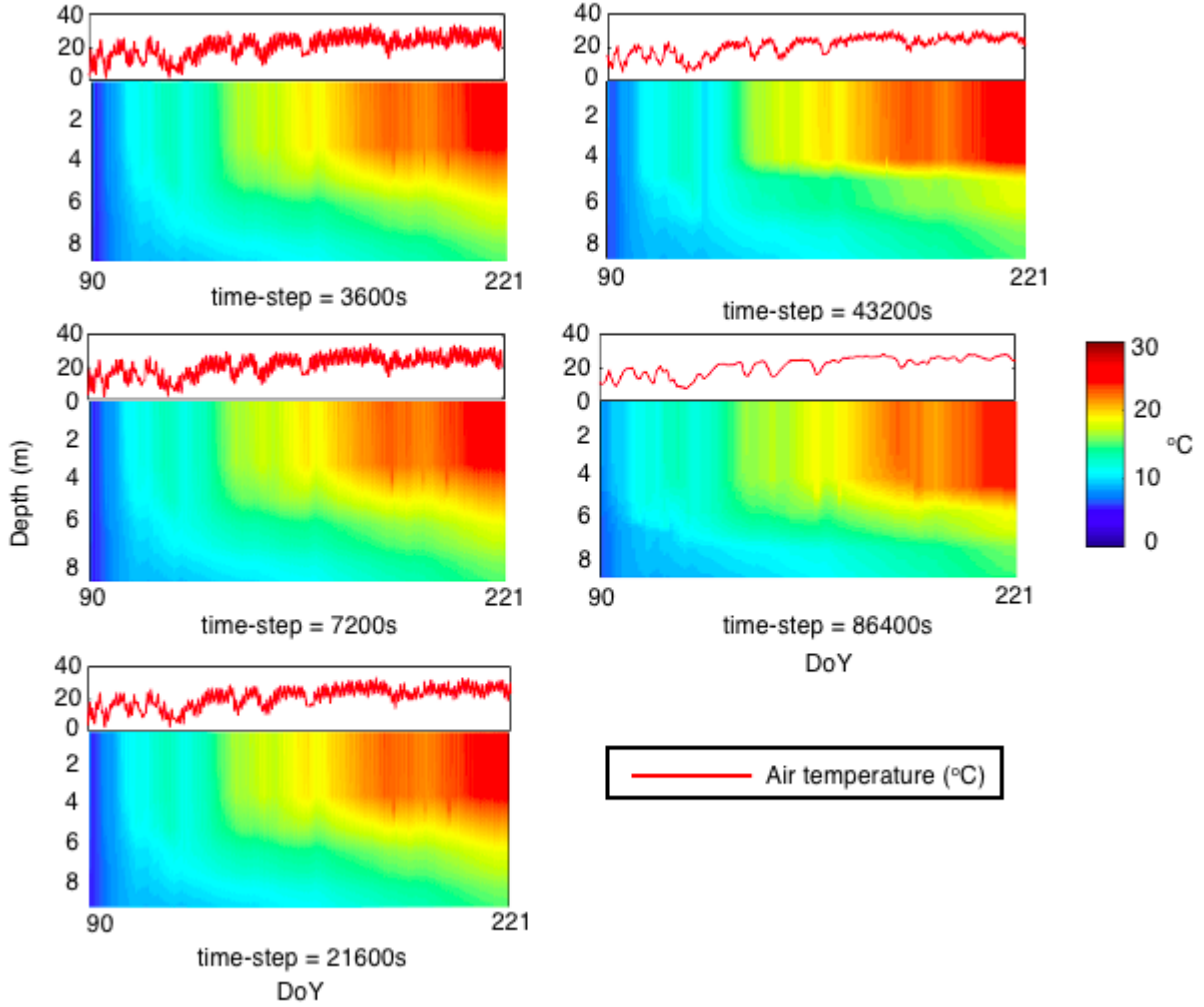


Figure S2. Temperature and input air temperature data plots of time-step dependence tests with the 1-D model (sediment module on) and input air temperature data.

Figure S1 presents the input meteorological data, which is available at 1-hour intervals. For time-steps longer than 1 hour, the meteorological data is averaged over the period of each time-step. As an example, the averaged air temperature conditions used in the GLM-AED2 simulations with the various time-steps are plotted in Figure S2 along with the modelling results of the temperature variations. A visual inspection indicates that the temperature plots do not substantially vary as the time-step is increased from 3,600s (1 hour) to 86,400s (1 day). To quantify the effect of the time-step on the model predictions, we calculate the thermocline depth and the metalimnion bottom depth, as illustrated in Figure S3(a), which plots the reservoir temperature structure in FCR on May 1st, 2015. Table S1 and Figure S3(b) compare the calculated average thermocline depths and metalimnion bottom depths over the stratified period using the 1-D model with the different time-steps. Thermocline is a layer with the largest density gradient and the metalimnion is the layer with the steepest thermal gradient in a stratified water body [36]. These physical indices reveal the lake response to heat budget and mixing dynamics. It is seen in Table S1 that the absolute variations of the numerical results obtained with the larger time-steps relative to the results obtained with the 3,600s (1 hour) time-step are $\leq 10\%$ for the average thermocline depth and $\leq 5.8\%$ for the average metalimnion bottom depth. Here, the absolute variations are calculated using Equation (S1):

$$absolute\ variation = \left| \frac{v_c - v_f}{v_f} \right| \quad (S1)$$

where v_f and v_c are respectively the variable of interest simulated with the finest mesh (or the smallest time-step) and that with the coarser mesh or larger time-step.

The relatively larger variation of the predicted average thermocline depth is observed because the thermocline depth is not as stable as the metalimnion bottom depth. The former is determined by both the surface heating and the water body mixing [S1], whereas the latter is only affected by the water body mixing. The present reservoir heat structure analysis confirms that a time-step between 3,600s (1 hour) and 86,400s (1 day) is appropriate for numerical simulations.

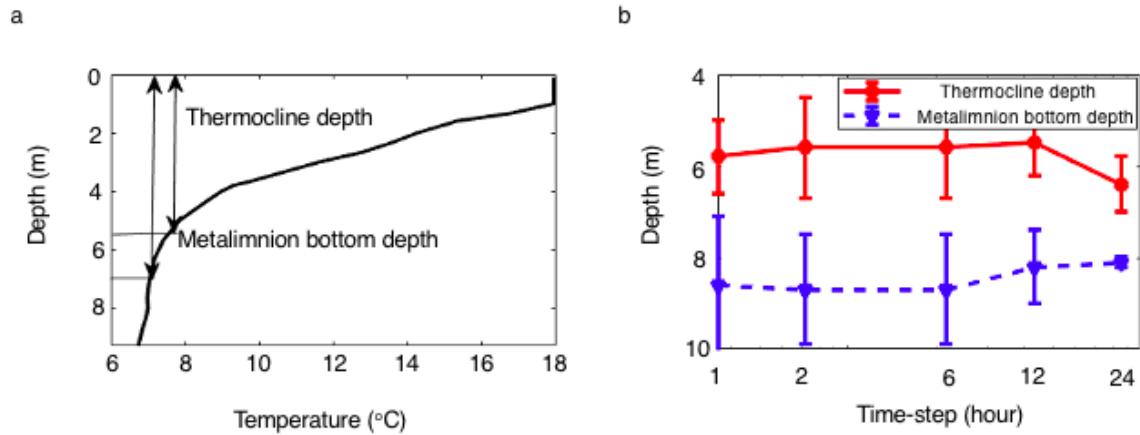


Figure S3. (a) A sketch of the temperature structure in FCR on May 1st, 2015; (b) 1-D model results of the average thermocline depths and metalimnion depths obtained with different time-steps. The error bars in figure (b) represent one standard deviation of uncertainty.

S2. Si3D-AED2 grid and time-step dependency test results

To quantify the sensitivity of the 3-D model predictions to the spatial and temporal resolutions, the monthly average thermocline depths and metalimnion bottom depths are calculated during the stratified period. For the mixed period, the average temperature over the full depths is calculated. Here, the time period between the spring and fall turnover is referred to as the stratified period, and the rest of the year is referred to as the mixed period. Spring and fall turnover is defined as the days when the temperature at 1m equals the temperature at 8m using observations made every 15 min throughout the monitoring period by two optical INW DO2 DO sondes (Seametrics, WA, USA) [46].

Table S2. Spatial resolution and time-step settings, the corresponding computing time and results at FCR50.

Test No.	1	2	3
Time-step (s)	2.5	5	10
Spatial resolution (m)	2.5×10×0.15	5×20×0.3	10×40×0.6
Cell numbers	85632	10704	1338
Computing time*	320min	60min	13min
Average thermocline depth in the stratified period (m)	5.7 ± 2.0	5.6 ± 1.7	5.5 ± 1.2
Absolute variation** (%)	–	1.8	3.5
Average metalimnion bottom depth in the stratified period (m)	7.7 ± 1.2	7.8 ± 1.2	8.1 ± 1.0
Absolute variation** (%)	–	1.3	5.2
Average temperature over all depths in the mixed period (°C)	17.5 ± 7.3	17.7 ± 7.3	18.1 ± 7.2
Absolute variation** (%)	–	1.1	3.4

* Wall clock time (real time) for a one-day simulation using 4× Intel Core i5-4570S CPU @ 2.90GHz.

** The average absolute variation is calculated relative to the finest mesh (2.5m×10m×0.15m) and the smallest time-step (2.5s) results.

Table S3. Cell resolution and time-step settings, the corresponding computing time and results at FCR45.

Test No.	1	2	3
Time-step (s)	2.5	5	10
Cell resolution (m)	2.5×10×0.15	5×20×0.3	10×40×0.6
Cell numbers	85632	10704	1338
Computing time*	320min	60min	13min
Average thermocline depth in the stratified period (m)	5.0 ± 1.2	4.7 ± 1.3	4.5 ± 1.0
Average absolute variation* (%)	–	6.0	10
Average metalimnion bottom depth in the stratified period (m)	7.3 ± 0.7	7.2 ± 0.8	7.1 ± 0.9
Average absolute variation* (%)	–	1.4	2.7
Average temperature over all depths in the mixed period (°C)	17.5 ± 7.3	18.0 ± 7.2	17.9 ± 7.2
Average absolute variation* (%)	–	0.6	1.7

* Wall clock time (real time) for a one-day simulation using 4× Intel Core i5-4570S CPU @ 2.90GHz.

** The average absolute variation is calculated relative to the finest mesh (2.5m×10m×0.15m) results.

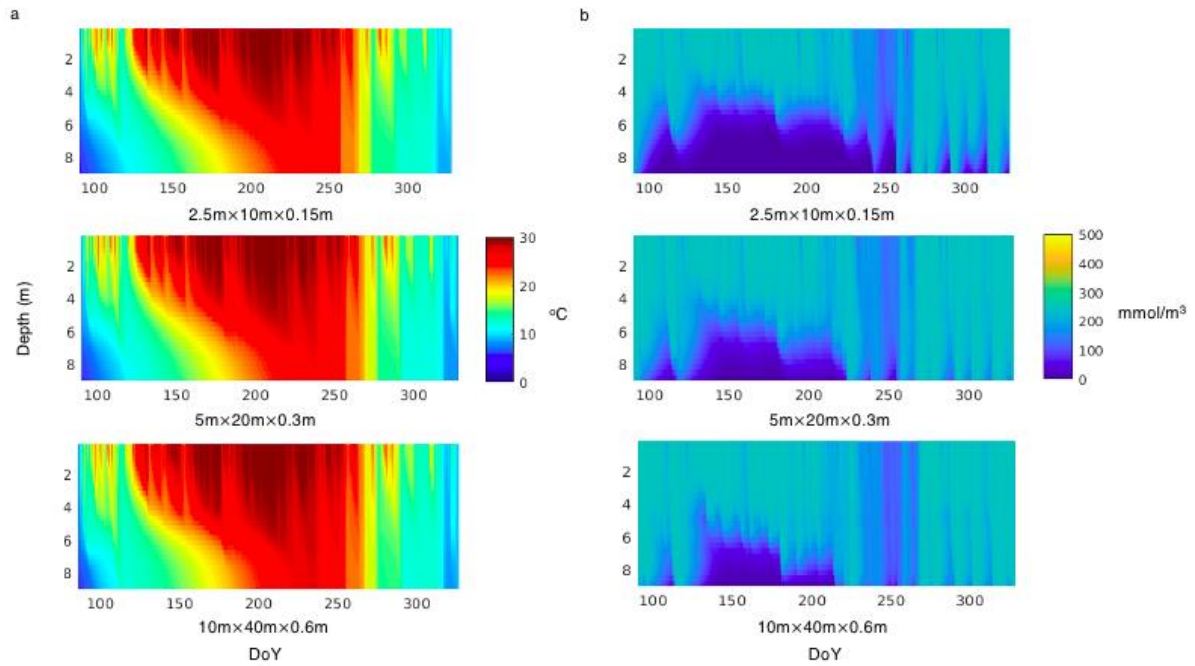


Figure S4. Results at FCR50 from the 3-D cell resolution and time-step dependence tests (a) Temperature; (b) Dissolved oxygen (DO).

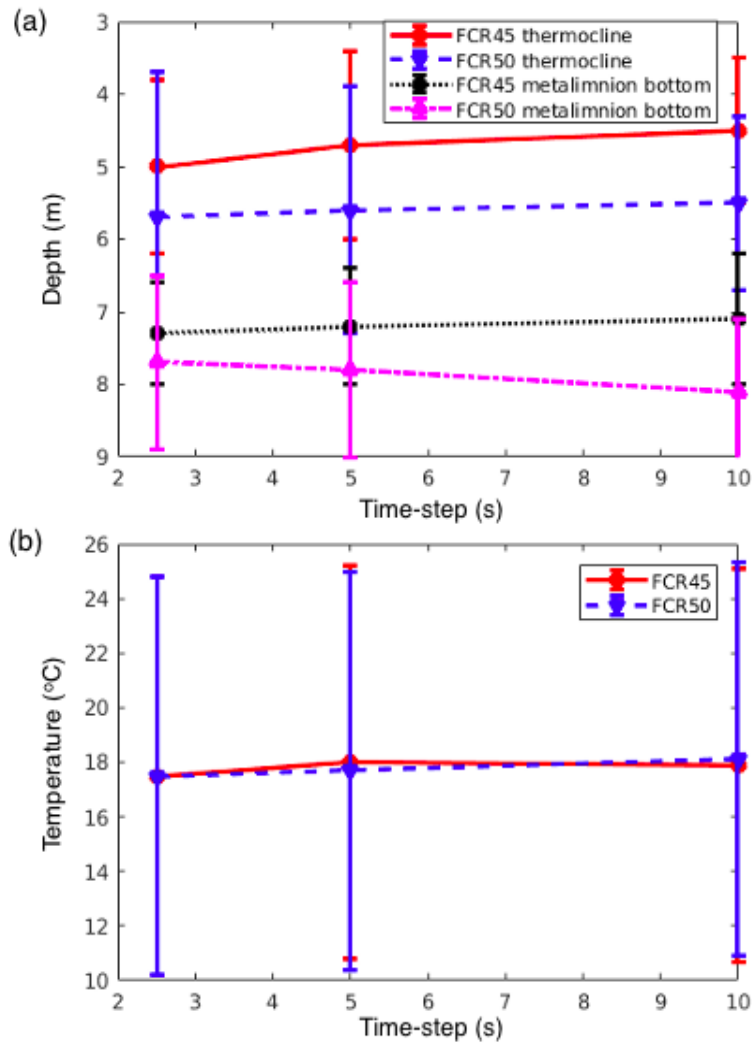


Figure S5. Results at FCR50 and FCR45 from the 3-D cell resolution and time-step dependence tests. (a) The average thermocline depths and metalimnion bottom depths during the stratified period. (b) The average temperature over the full depth during the mixed period. The error bars in figure (b) represent one standard deviation of uncertainty.

Table S2 (see also Table S4) shows the time-steps, cell sizes and the corresponding computing time of the numerical tests. Figures S4(a) and (b) show the temperature and DO concentration profiles obtained with the 3-D model using the different cell sizes and time-steps. From visual inspection of Figure S4(a) and (b), as the cell is refined from 10m×40m×0.6m to 2.5m×10m×0.15m, the area of dark colour in the temperature profiles (whose temperature is more than 30 °C) decreases while the height of the anoxic zone presented in the DO concentration profiles developed between DoY 100 – 250 increases. In spite of these minor differences, all three sets of test results have similar thermal structures during the stratified period.

Figures S5(a) (see also Table S2 and Table S3) presents the average thermocline depths and metalimnion bottom depths in the stratified period, and Figure S5(b) (see also Table S2 and Table S3) presents the average temperature over the full depth during the mixed period. It can be observed in Figure S5(a) and (b) that the predicted average thermocline depth, the metalimnion bottom depth over the stratified period and the average temperature across the full depths over the mixed period at FCR45 and FCR50 all converge with reducing cell sizes. It should be noted that, in the shallower regions of the

reservoir (e.g. FCR10, FCR20, FCR30), water body stratification is not developed during the simulation period, and thus only the results at FCR45 and FCR50 are presented.

S3. GLM-AED2 Sediment Heat Module Test

The GLM-AED2 sediment module is turned on for the above-described time-step dependence test. Additional tests are performed to evaluate the impact of the sediment heat module on the simulation results. In this section, the Year 2014 and 2015 simulation results with and without sediment heat module are presented.

To evaluate the performance of the models, the RMSEs of the temperature and DO are calculated using Equation (S2):

$$RMSE = \sqrt{\frac{\sum_1^n (v_{field} - v_{sim})^2}{n}} \quad (S2)$$

where v_{field} and v_{sim} are respectively the field measurement and simulated data of the variable of interest, and n is the total number of field data points. Here, we examine the whole-lake RMSEs of the temperature and DO, which are presented in Table S4.

Table S4. The whole-lake RMSEs of the predicted temperatures (in °C) and DO (in mmol/m³) for Year 2014 and 2015 with GLM-AED2 sediment module on and off. The lower RMSEs between the sediment module on and off results are shown in bold.

	Sediment module on		Sediment module off	
	Temperature (°C)	DO (mmol/m ³)	Temperature (°C)	DO (mmol/m ³)
2014	1.99	72.8	3.10	144.2
2015	1.86	90.5	2.36	141.8

In Table S4, substantially lower whole-lake temperature and DO RMSEs in GLM-AED2 simulations after turning on the sediment module are observed for both Year 2014 and 2015. One typical example is the temperature RMSE in Year 2014, which decreases by more than 35% by activating the sediment module.

To quantify the amount of heat transferred from the water body to the sediment, the rates of the temperature change caused by sediment/water heat exchange at the water surface and at the metalimnion from the GLM-AED2 simulation of Year 2015 are presented in Figure S6. The rate of the temperature change for each layer caused by sediment/water heat exchange is calculated from Equation (S3) [32], where A is the area, c_w is the specific heat capacity of water, K_{soil} is the soil-sediment thermal conductivity, T_z is the temperature of the sediment, T is the water temperature, V is the volume, ρ is the density, δz_{soil} is the length scale associated with the heat flux, and subscript ' i ' refers to quantities of the i^{th} layer. Among these, K_{soil} and δz_{soil} are input parameters.

$$c_w \rho_i V_i \frac{dT_i}{dt} = K_{soil} \frac{(T_{z_i} - T_i)}{\delta z_{soil}} (A_i - A_{i-1}) \quad (S3)$$

It can be observed in Figure S6 that a significant amount of heat transfer between water and sediment occurs in GLM-AED2 during Year 2015 simulation, with the corresponding daily temperature change rate varying from 1 °C/d to -1 °C/d. This explains the significant improvement in GLM-AED2 temperature and DO results after turning on the sediment heat module.

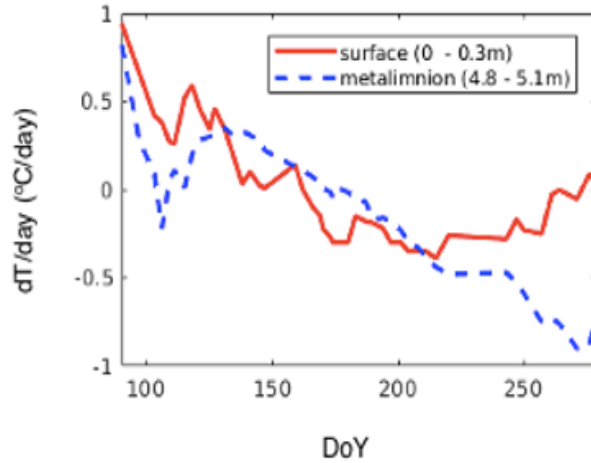


Figure S6. Temperature variation due to sediment/water heat exchange at the water surface (0 – 0.3m) and at the metalimnion (4.8 – 5.1m) from the GLM-AED2 Year 2015 simulation.

S4. Plume Detrainment Location Tests

Both GLM-AED2 and Si3D-AED2 have two detrainment options for the coupled bubble plume models, denoted by DNB and DMPR, respectively, meaning detrainments at the depth of neutral buoyancy and the depth of maximum plume rise, respectively. Figure S7 shows the schematic diagrams of the two variants of bubble plume models that are tested here. Based on the well-established bubble plume modeling theory [12,19, S2,39], the buoyant plume is created by air bubbles injected from the diffuser line within the metalimnion. During the rise of the plume, it entrains ambient water with momentum that carries it past the DNB to reach the DMPR [20, S3]. Subsequently, the plume water falls back and intrudes near the DNB [S4, S5]. Three sets of EM experiments performed in FCR in Year 2016, the details of which have been given in Table 2, are simulated using these two bubble plume model variants coupled with GLM-AED2 and Si3D-AED2, respectively. The RMSEs of the simulated metalimnion bottom depths are calculated to evaluate model performances (Table S4).

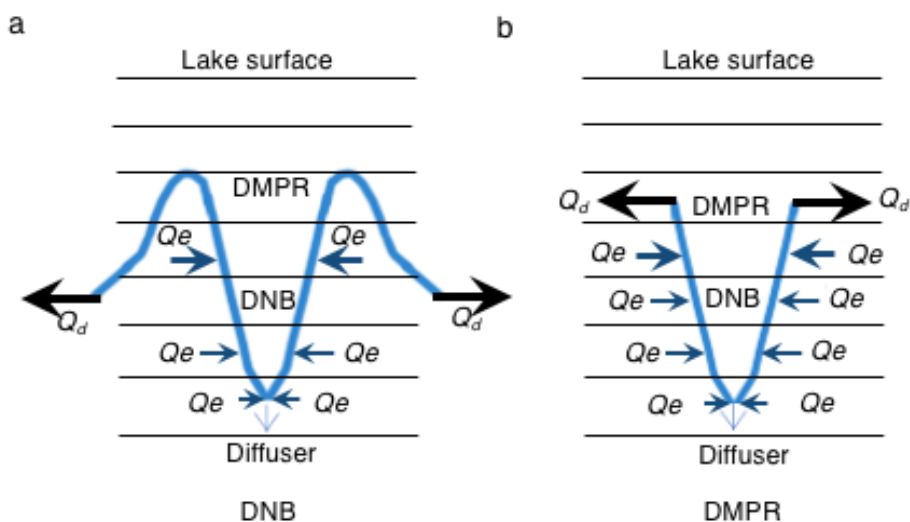


Figure S7. Schematic diagram of the bubble plume model variants (a) DNB (b) DMPR. DNB refers to detrainment at the depth of neutral buoyancy point, and DMPR refers to detrainment at the depth of maximum plume rise.

Table S4. RMSEs (in m) of the simulated metalimnion bottom depths during the EM periods of Year 2016.

	EM1	EM2	EM3	Weighted average
GLM_DNB	0.6	1	0.7	0.7
GLM_DMPR	0.9	1.2	0.7	0.9
Si3D_DNB	0.2	0.9	0.4	0.5
Si3D_DMPR	0.3	1	0.3	0.6

Table S4 shows that GLM_DNB consistently has lower or equal RMSEs in all three simulations than GLM_DMPR. For Si3D, the situation is slightly different. Si3D_DNB has lower RMSEs for EM1 and EM2, but higher RMSEs for EM3. In terms of the weighted average, GLM_DNB and Si3D_DNB respectively outperform GLM_DMPR and Si3D_DMPR. The better performance of GLM_DNB and Si3D_DNB indicates that detrainning plume water at the neutral buoyancy point is more reasonable for both GLM and Si3D than detrainning plume water at DMPR. A possible explanation of the variations is that detrainning plume water at DNB better accounts for the near-field recirculation [S5].

References

- S1. Hambright, K.D., Gophen, M., Serruya, S., 1994. Influence of long-term climatic changes on the stratification of a subtropical, warm monomictic lake. *Limnol. Oceanogr.* 39(5), 1233-1242.
- S2. Singleton, V.L., Rueda, F.J., Little, J.C., 2010. A coupled bubble plume–reservoir model for hypolimnetic oxygenation. *Water. Resour. Res.* 46(12).
- S3. McDougall, T.J., 1978. Bubble plumes in stratified environments. *J. Fluid. Mech.* 85(4), 655-672.
- S4. Morton, B.R., Taylor, G., Turner, J.S., 1956. Turbulent Gravitational Convection from Maintained and Instantaneous Sources. *Proc. R. Soc. Lond. A* 234:1-23. <http://doi.org/10.1098/rspa.1956.0011>
- S5. Socolofsky, S.A., Bhaumik, T., Seol, D., 2008. Double-plume intergral models for near-field mixing in multiphase plumes. *J. Hydraul. Eng.* 134(6), 772-783.